Electronic Supplementary Material (ESI) for Physical Chemistry Chemical Physics.

Supplementary Information

DFT study on Ag loaded 2H-MoS_2 for mechanism of improved photocatalytic reduction of CO_2

Tianwei Ouyang[a], Wenyuan Fan[a], Jiaqing Guo[a], Yinan Zheng[a], Xiaohong Yin[*a] and Yongli Shen[*b]

[a]Tianjin Key Laboratory of Organic Solar Cells and Photochemical Conversion, School of Chemistry and Chemical Engineering, Tianjin University of Technology, Tianjin 300384, China

[b]Tianjin Key Laboratory of Advanced Functional Porous Materials, Institute for New Energy Materials & Low-Carbon Technologies, School of Materials Science and Engineering, Tianjin University of Technology, Tianjin 300384, China

Corresponding authors

*E-mail: yinxiaohong@tjut.edu.cn

*E-mail: ylshen@tjut.edu.cn

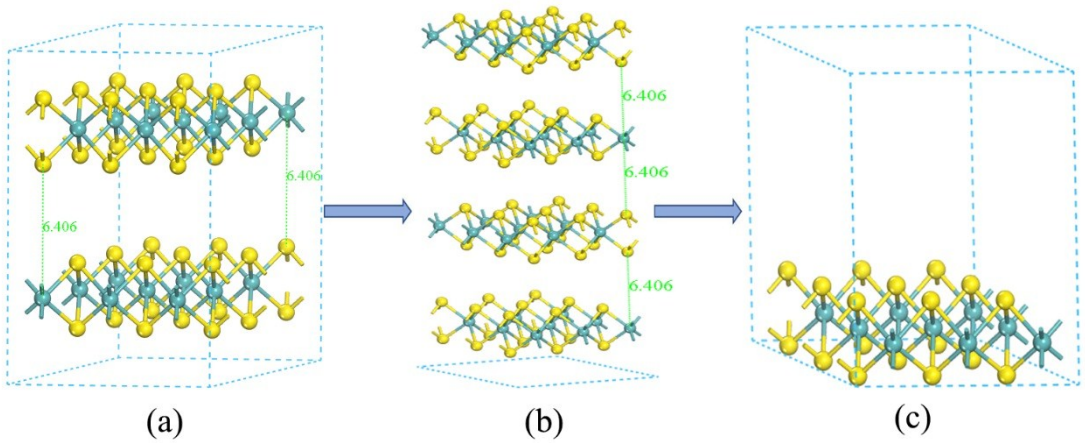

Figure S1. (a) the geometry structure of bulk 2H-MoS_2, (b) the multilayer structure of 2H-MoS_2 (002), and (c) the single-layer nanosheet structure of 2H-MoS_2.

As shown in **Figure S1**, the symmetry of our choice of molybdenum disulfide is P_{63}-mmc, which is a stable 2H semiconductor state [1]. The interlayer distance of 2H-MoS_2 after full optimization is 6.406 Å, which is consistent with previous reports [2,3]. In our experiments, 2H-MoS_2 (002) has the best photocatalytic activity and the Ag nanoparticles were approximately 100-200 Å in average diameter [4]. Considering the possibility of preparing much smaller nanoparticles, we tracked the Ag preparation methods and found the diameter of Ag nanoparticles prepared by chemical reduction of citric acid to be at 40-800 Å [5]. These diameters of Ag nanoparticles are much larger than the interlayer distance of 2H-MoS_2 (002). Therefore, Ag nanoparticles cannot enter 2H-MoS_2. Based on the above analyses, this work chooses loading Ag atoms on a single layer of 2H-MoS_2 nanosheets.

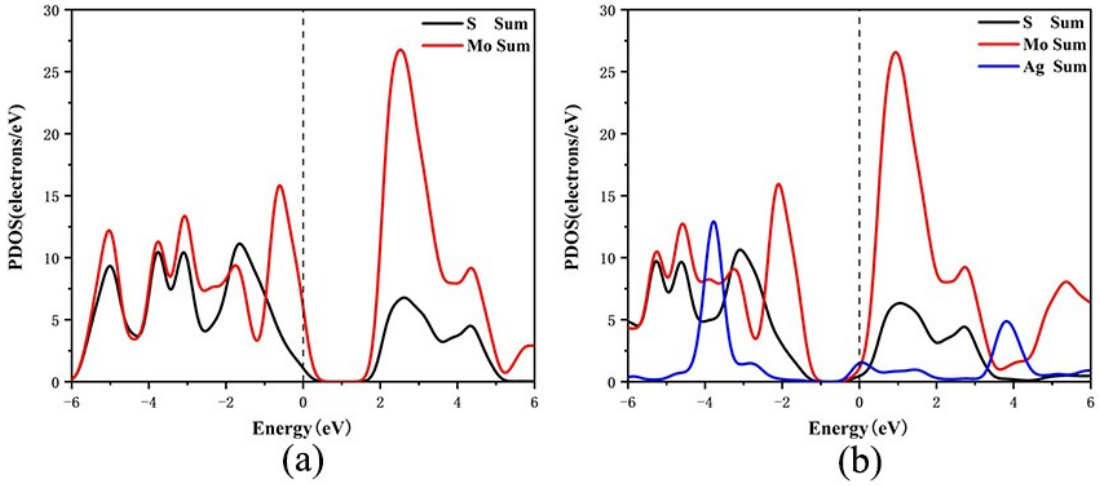

Figure S2. PDOS of (a) 2H-MoS_2 and (b) Ag/2H-MoS_2.

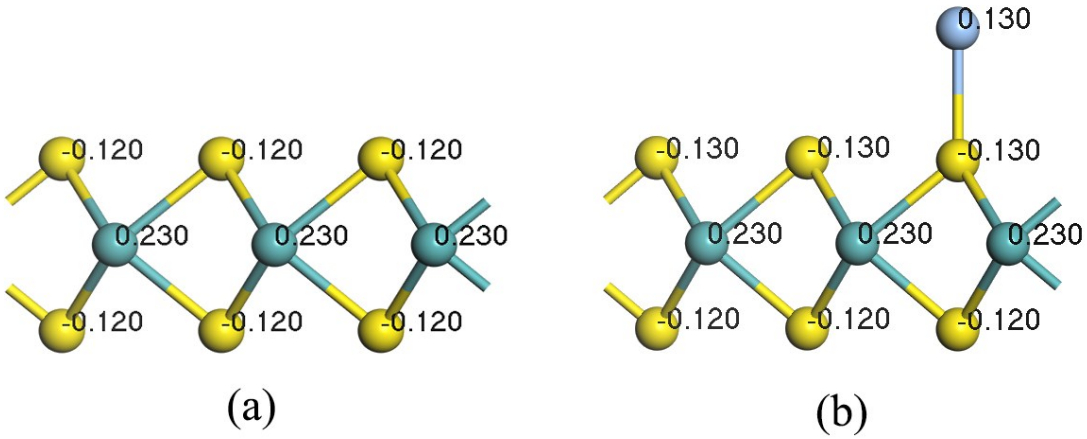

Figure S3. Hirshfeld charges population to (a) 2H-MoS_2, (b) Ag/2H-MoS_2 in a 3×3×1 supercell. Yellow: sulfur, blue: molybdenum, and gray: silver.

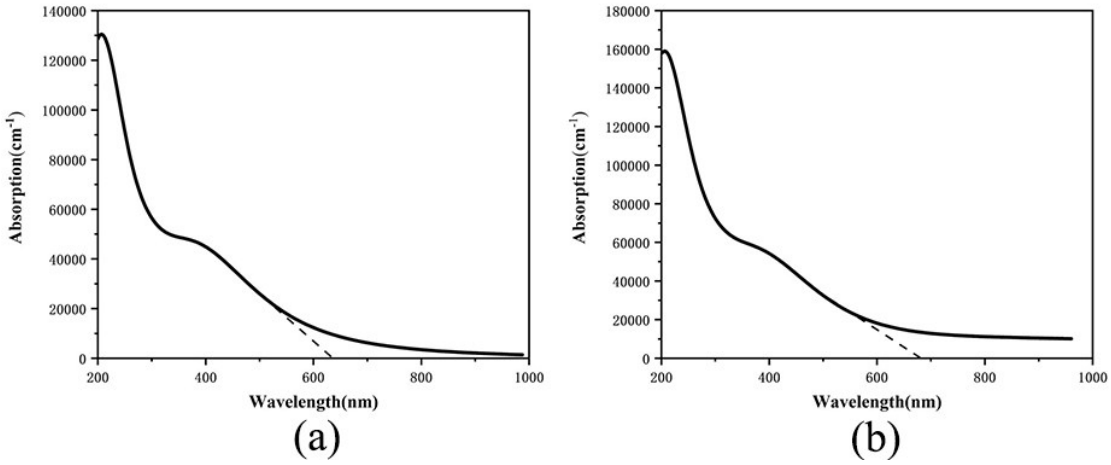

Figure S4. Optical absorption behaviors of (a)2H-MoS_2 and (b)Ag/2H-MoS_2.

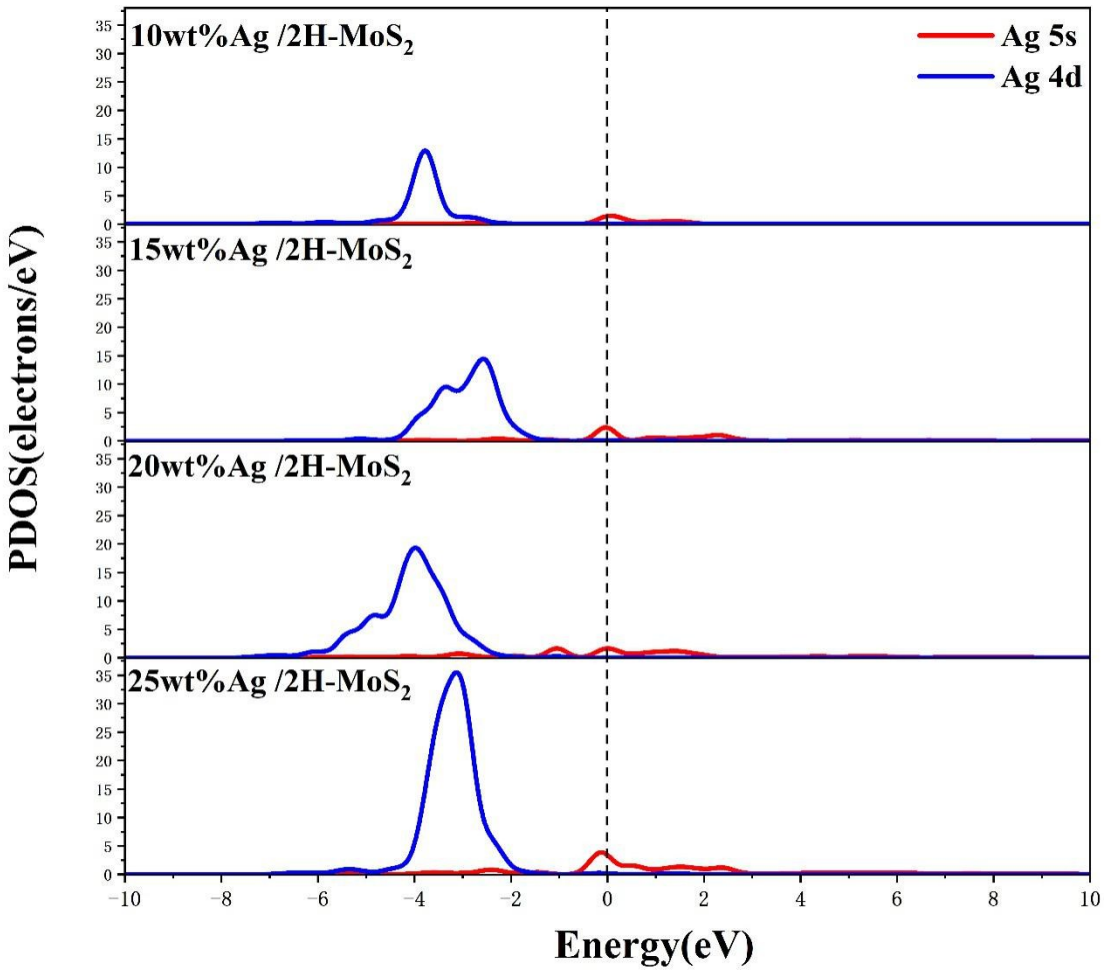

Figure S5. PDOS of different loadings of Ag atoms on 2H-MoS_2.

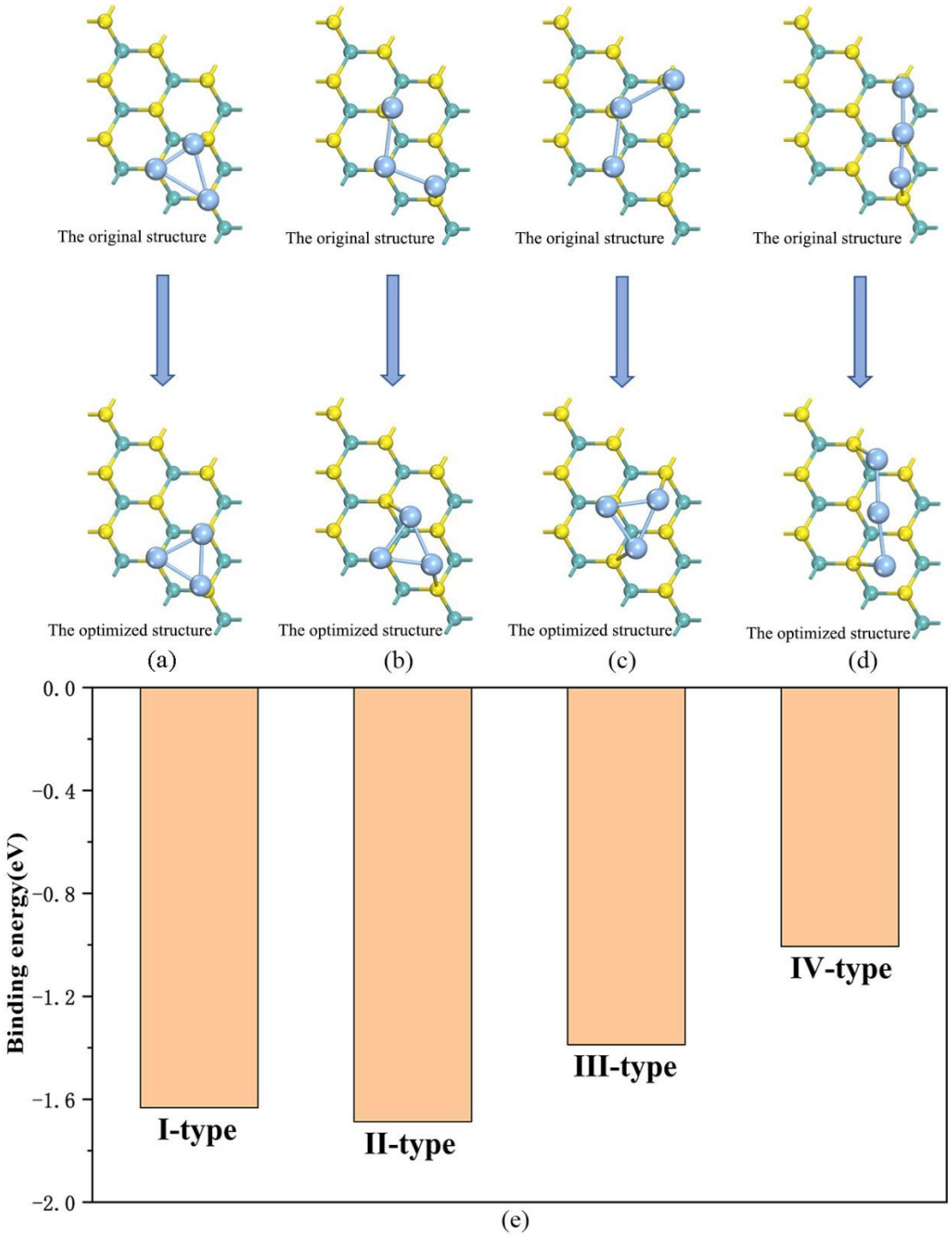

Figure S6. 20wt% Ag/2H-MoS_2 structural model of (a) I-type, (b) II-type, (c) III-type, (d) IV-type. (e) The binding energy needed to form four stable structures.

We construct four structures as I-type, II-type, III-type and IV-type for 20wt% Ag/2H-MoS_2 and show them in **Figure S6(a)-(d)**. Among them, I-type is a structure of three Ag atoms in triangular arrangement, II-type and III-type are polyline structures, and IV-type has a structure of three Ag atoms in line. It is worth noting that II-type and III-type also change to the triangular arrangement after the structure optimization, so the triangular structure is more stable than the polyline structure. Our calculation results show that the binding energies required to form I-type and II-type are very similar, respectively -1.633 eV and -1.687 eV, as shown in **Figure S6 (e)**, the difference is only

0.054 eV. But after the structure optimization, there are only two Ag-S bonds in the three Ag atoms of II-type, so we explored the bond populations and bond lengths of I-type and II-type in **Table S4**, where the bond populations of the three Ag-S bonds and the bond lengths in I-type are relatively uniform and stable at about 2.7Å, respectively. However, the three Ag atoms in the II-type interacted with the four nearby S atoms, and their bond populations of Ag 1- S 12 and Ag 2- S 4 are 0.03 and 0.05 respectively, which are obviously smaller than those of the rest Ag-S bonds. Thus, it is reasonable to speculate some chemical bonds in II-type are weaker than those in I-type. Additionally, the bond lengths of Ag 1- S 12 and Ag 2- S 4 in II-type are also extended to 2.9Å, which makes these Ag-S bonds in II-type to be easier to break, thus the II-type seems only two chemical bonds between three loaded Ag atoms and the 2H-MoS_2 carrier. In summary, I-type is conducive to the stability of the structure. Therefore, we abandoned II-type and chose to use I-type in our work for follow-up research.

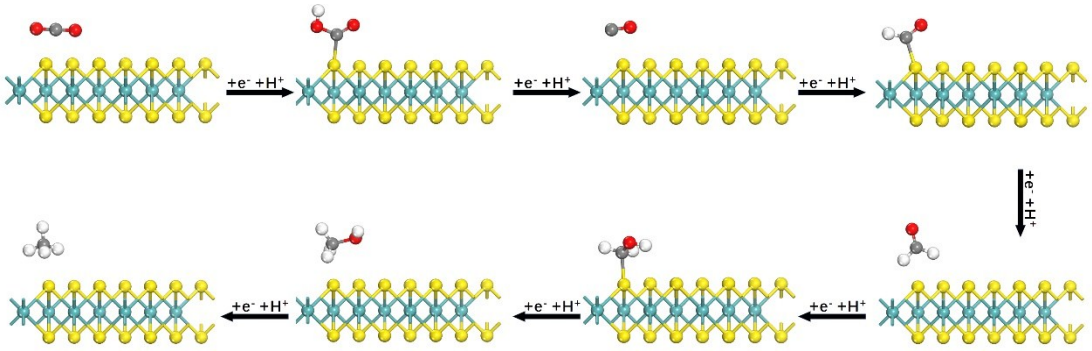

Figure S7. Structural model corresponding to FH path of 2H-MoS_2.

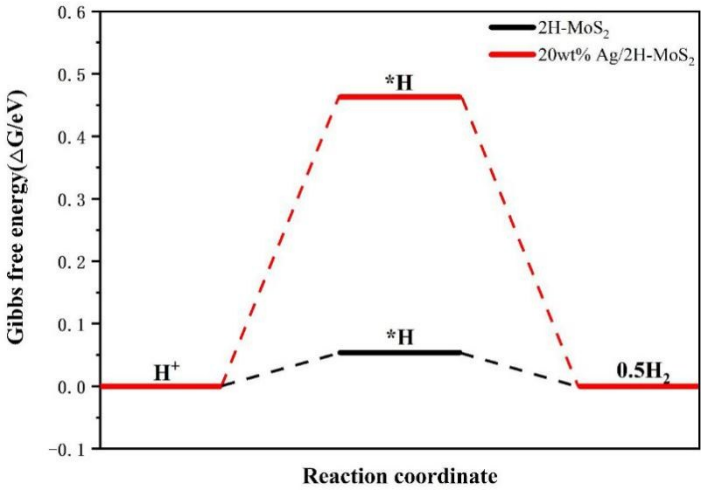

Figure S8. Gibbs free energy of hydrogen evolution reaction (HER) on 2H-MoS_2 and 20wt%Ag /2H-MoS_2.

As shown in **Figure S8**, The Gibbs free energy changes of the HER [6,7] on 2H-MoS_2 and 20wt% Ag/2H-MoS_2 are lower than that of the potential-limiting step of CO_2 reduction, manifesting that the HER side reaction are easier to perform in low pH areas. However, it is experimentally possible to prevent HER by adjusting the pH of the electrolyte or using a non-aqueous solvent such as acetonitrile, DMF, etc. [8]. Therefore, the effects of the HER side reaction are minimized through regulation in the experiment.

Table S1. The ratio of the number of atoms based on the weight ratio and molar ratio of Ag atoms to S atoms in the experiment

Composite	10wt% Ag/2H-MoS_2	15wt% Ag/2H-MoS_2	20wt% Ag/2H-MoS_2	25wt% Ag/2H-MoS_2
Weight Ratio	0.1	0.15	0.2	0.25
Molar ratio	0.148	0.223	0.297	0.371
Atomic Ratio	1.332	2.007	2.672	3.339

Table S2. Calculated Gibbs free energies of CO_2 reduction into CH_4 on 2H-MoS_2 and 20wt%Ag /2H-MoS_2 in the fast hydrogenation (FH) pathway.

Intermediate products	**Gibbs free energy (eV)**	
	2H-MoS_2	20wt%Ag /2H-MoS_2
Surface+ CO_2	-0.299	-0.272
Surface+*COOH	2.395	0.653
Surface+*CO	-1.605	-0.272
Surface+*COH	3.075	2.313
Surface+*CHO	1.225	0.653
Surface+*CHOH	0.653	0.680
Surface+*CH_2O	-1.524	-0.680
Surface+*OCH_3	1.333	-0.354
Surface+*CH_2OH	0.844	0.245
Surface+*CH_3OH	-1.714	-0.599
Surface+*CH_3	0.653	0.245
Surface+ CH_4	-1.442	-1.143

Table S3. Calculated Gibbs free energies of CO_2 reduction into CH_4 on 2H-MoS_2 and 20wt%Ag /2H-MoS_2 in the fast deoxygenation (FO) pathway.

Intermediate products	**Gibbs free energy (eV)**	
	2H-MoS_2	20wt%Ag /2H-MoS_2
Surface+ CO_2	-0.299	-0.272
Surface+*COOH	2.395	0.653
Surface+*CO	-1.605	-0.272
Surface+*C (FO)	4.299	3.701
Surface+*CH (FH)	-1.605	-1.742
Surface+*CHO	1.225	0.653
Surface+*CH (FO)	1.469	1.306
Surface+*CH_2 (FH)	-2.014	-1.986
Surface+*CH_3	-1.197	-0.708
Surface+*CH_3OH	-0.653	-0.245
Surface+ CH_4	-2.095	-1.388

Table S4. Bond populations and lengths of I-type and II-type for 20wt% Ag/2H-MoS_2.

Load configuration	Bond	Population	Length(Å)
20wt% Ag/2H-MoS_2 of I-type	Ag 1- S 6	0.14	2.737
	Ag 2- S 4	0.11	2.742
	Ag 3- S 12	0.13	2.766
20wt% Ag/2H-MoS_2 of II-type	Ag 1- S 10	0.12	2.856
	Ag 1- S 12	0.03	2.920
	Ag 2- S 4	0.05	2.921
	Ag 3- S 6	0.14	2.794

References

1 Zongyan Zhao, Qinglu Liu, Catal. Sci. Technol., 2018, 8, 1867-1879.

2 X. Zhang, W. P. Han, J. B. Wu, S. Milana, Y. Lu, Q. Q. Li, A. C. Ferrari, P. H. Tan, Phys. Rev. B., 2013, 87, 115413.

3 Jiangang He, Kerstin Hummer, Cesare Franchini, Phys. Rev. B., 2014, 89, 075409.

4 Yinan Zheng, Xiaohong Yin, Yue Jiang, Junsong Bai, Yuan Tang, Yongli Shen, Ming Zhang, Energy Technol., 2019, 1900582.

5 Yu Wana, Zhirui Guo, Xiaoli Jiang, Kun Fang, Xiang Lu, Yu Zhang, Ning Gu, J. Colloid Interf. Sci., 2013, 394, 263-268.

6 Yawei Li, Haibin Su, Siew Hwa Chan, Qiang Sun, ACS Catal., 2015, 5, 11, 6658-6664.

7 Haoming Shen, Yawei Li, Qiang Sun, J. Phys. Chem. C., 2017, 121, 3963-3969.

8 Klaas Jan P.Schouten, ElenaPérez Gallent, Marc T.M.Koper, J. Electroanal. Chem., 2014, 716, 53-57.